Electrochemistry Communications 60 (2015) 109–112

Contents lists available at ScienceDirect

Electrochemistry Communications

journal homepage: www.elsevier.com/locate/elecom

Short communication

Easily prepared, high activity Ir–Ni oxide catalysts for water oxidation

Reza B. Moghaddam [a,b], Chao Wang [a], Jason B. Sorge [b], Michael J. Brett [b], Steven H. Bergens [a,*]

[a] Department of Chemistry, University of Alberta, Edmonton, AB, T6G 2G2, Canada
[b] Department of Electrical and Computer Engineering, University of Alberta, Edmonton, AB, T6G 2V4, Canada

ARTICLE INFO

Article history:
Received 23 July 2015
Received in revised form 19 August 2015
Accepted 19 August 2015
Available online 22 August 2015

Keywords:
Water oxidation
Oxygen evolution
Iridium
Nickel
Water electrolyzer

ABSTRACT

Ir–Ni oxide nanoparticles were simply prepared by stirring $IrCl_3$ and $NiCl_2$ precursors in aqueous base under air. The activities of a series of $IrNi_yO_x$ nanoparticles with different Ir-to-Ni ratios were measured toward water oxidation in 0.1 M H_2SO_4. The Ir-to-Ni ratio was 1:0.125 in the most active catalyst (mass normalized > 140 A g^{-1} Ir, electrochemically active surface area normalized > 203 A $mmol^{-1}$Ir). The stabilized potential for the galvanostatic oxidation (1 mA $cm^{-2}_{geometric}$) was as low as 1.51 V_{RHE}, corresponding to 0.28 V in overpotential.

1. Introduction

Renewable energy systems such as photovoltaic devices [1–3] require that electrical energy be efficiently stored and released. A promising method to store electrical energy on large scales is the electrolysis of water [4–6]. The resulting hydrogen can be converted back into electricity with fuel cells (*e.g.* proton exchange membrane fuel cells, PEMFC) [7–9]. The water oxidation reaction (WOR) at the anode of an electrolyser requires an electrocatalyst [10–14]. While the standard potential for the WOR (E°) is 1.23 V_{RHE}, the kinetics of the WOR are slow, resulting in significant anode overpotentials in water electrolyzers [11]. Many single and multicomponent metallic catalysts have been investigated to accelerate the WOR in acid [10–13,15–18]. Catalysts containing Ir (regarded as derivatives of Ir(IV)-oxo species) have the most favorable combination of activity and stability in acid to date. Catalysts containing Ru are also active, but Ru is not stable to prolonged operation at WOR potentials in acid [19,20]. As a result, Ir-oxide nanoparticles are presently the benchmark for the WOR in acid [21], and much of the research in this area is directed toward optimizing the utilization of Ir [10,12,21–25]. For example, Berlinguette *et al.* recently published a photochemical decomposition of Ir(acetylacetonate)$_3$ deposits to form amorphous IrO_x films that were active toward the WOR in acid [22]. Among the more active acid WOR catalysts are those reported by Strasser *et al.* [10–13]. With a series of dealloyed Ir-oxide core-shell catalysts, they obtained mass activities in acid as high as ~ 40 A g^{-1} at 0.25 V overpotential [10]. The most active IrNi@IrO_x catalyst in this series was three times more active than the pure Ir. More recently, this group reported a mass activity of ~90 A g^{-1} Ir, with $E_{working} = 1.51$ V_{RHE}, using a $IrNiO_x$ catalyst on antimony-doped tin oxide annealed at 180 °C [11].

Colloidal suspensions of IrO_x nanoparticles (NPs) typically contain organic stabilizers that protect the surface of the oxide particles [26–30]. In 2010, Berkerman reported [17] that small (~1 nm) IrO_x NPs could be prepared in relatively high concentrations as stable suspensions in water by a simple, bench top reaction between $IrCl_3$ and hydroxide solutions in the presence of oxygen. For this study, we adopted this methodology to prepare colloidal $IrNi_yO_x$ NPs suspensions. The NPs are characterized and were found to be remarkably active toward the WOR in acid.

2. Experimental

2.1. Chemicals

Sulfuric acid (Alfa Aesar; 99.9999%), potassium hydroxide (Aldrich; semiconductor grade, 99.99%), iridium chloride trihydrate (A.B. Mackay Chemicals), nickel chloride (Alfa Aesar; anhydrous, 98%), and Nafion (5 wt%, ElectroChem, Inc.) were used as received. Triply distilled water (last distillation from alkaline $KMnO_4$ solution) was used throughout the experiments.

2.2. Preparation of nanoparticle solutions

Colloidal suspensions of the mixed metal oxide NPs were prepared by modifying the procedure described for iridium oxides [17]. To prepare a pure Ir-oxide NP suspension (IrO_x NP), 0.0704 g $IrCl_3.3H_2O$ was dissolved in 20 mL water (*i.e.* 0.01 M solution of Ir^{3+}) to form a

* Corresponding author. Tel.: +1 780 492 9703.

http://dx.doi.org/10.1016/j.elecom.2015.08.015
1388-2481/

dark brown solution. Then, 2 mL of 1 M KOH diluted to 2.5 mL was added dropwise over 5 min. Upon adding the KOH, the dark brown color changed first to green, and then to blue after 2 days. The color did not change afterward. The IrO_x NP solution was then stored at room temperature. Control experiments (voltammetry in 0.1 M H_2SO_4) confirmed that the IrO_x NP suspension was stable for about 2 months at room temperature. $IrNi_yO_x$ (y: initial Ni^{2+}/Ir^{3+} molar ratio) mixed NP were prepared by adding 1 M KOH to 20 mL solutions of $IrCl_3$ and $NiCl_2$ in the weights and volumes shown in Table 1. The molar ratios of the precursor mixtures were $IrNi_{0.06}$, $IrNi_{0.125}$, $IrNi_{0.25}$, $IrNi_{0.5}$, and $IrNi_{1.0}$. There was no visual evidence of a precipitate after several weeks for the suspensions with y = 0–0.125. Precipitates formed from suspensions with y ≥ 0.25 after several days.

2.3. Preparation of working electrodes

The IrO_x or $IrNi_yO_x$ NP suspensions were diluted by a factor of five using water that contained the appropriate amounts of Nafion to give a final 1% wt. Nafion per total mass of Ir + Ni, calculated from the amounts in Table 1. Using a micropipette and graded microtips, 10 μL of the NP/Nafion suspension (sonicated for 2 min) was drop coated onto a bare glassy carbon (GC; 0.196 cm^2) electrode. The ink was dried over 20 min at 60 °C then left at room temperature for 20 min. To check the accuracy of the metal weighing, aliquots of the NP suspensions (for IrO_x and $IrNi_1O_x$) that nominally contained 3.4 μg Ir were analyzed by ICP-MS. The accuracy of the nominal mass was ~95% that of the actual ICP-MS value.

The electrochemical experiments were performed with a Solartron SI 1287 Electrochemical Interface controlled by CorrWare for Windows Version 2-3d software. The reference electrode was a saturated calomel electrode (SCE; Fisher Scientific); however, all potentials in this paper are reported versus reversible hydrogen electrode (RHE). A graphite rod formed the counter electrode. Uncompensated resistance was estimated by impedance (20 Ω) and corrected for. SEM was performed with a Hitachi S-4800 instrument. A JEOL 2011 transmission electron microscope (The Microscopy and Microanalysis Facility, University of New Brunswick) was used for TEM analysis. Samples for the inductively coupled plasma–mass spectrometry (ICP-MS) analysis were dissolved in 0.3 M HNO_3 and measured with Perkin Elmer Elan 6000.

3. Results

Fig. 1 shows the SEM (A, on GC with Nafion) and TEM (B, on Cu grid) of the IrO_x NPs. The average particle size, ~1 nm, and the dispersion were consistent with those reported previously [17]. Fig. 1(C) shows the voltammetric profile (0–1.25 V_{RHE}, 50 mV s^{-1}) of the IrO_x NP/Nafion deposit on GC in 0.1 M H_2SO_4. The profile contains Ir(III)–Ir(IV) redox peaks at 1.07 (anodic) and 0.93 V_{RHE} (cathodic) [31], along with other oxidation and reduction processes that are evident from the ill-defined shoulders on both directions. There are no hydrogen signals, indicating that metallic Ir is absent from the deposit. Fig. 1D shows the WOR activity of the IrO_x NP deposit (with 3.4 μg Ir) in the extended anodic range in 0.1 M H_2SO_4. The oxidation onset is ~1.42 V_{RHE}, corresponding to ~0.19 V overpotential. The mass-corrected WOR activity at 1.48 V_{RHE} (*i.e.* 0.25 V overpotential) is ~93 A g^{-1} Ir.

Table 1
Amounts used for the synthesis of the IrO_x and $IrNi_yO_x$ NPs.

Ir/Ni ratio	$IrCl_3$ / g	$NiCl_2$ / g	Added KOH (1 M) / mL
Ir	0.0597	–	2
$IrNi_1$	0.0599	0.0259	4
$IrNi_{0.5}$	0.0596	0.0130	3
$IrNi_{0.25}$	0.0597	0.0065	2.5
$IrNi_{0.125}$	0.0597	0.0032	2.25
$IrNi_{0.06}$	0.0597	0.0016	2.15

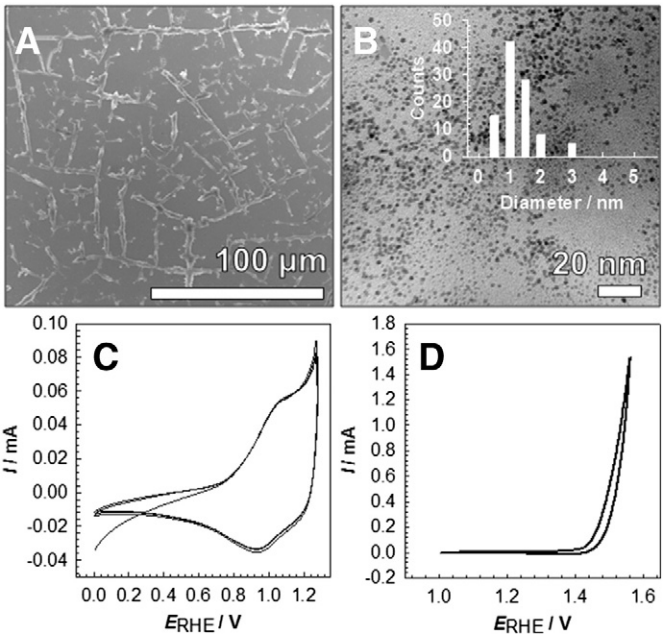

Fig. 1. SEM (A; on GC), TEM (B; on a Cu grid), and voltammetric profiles in 0.1 M H_2SO_4 at 50 mV s^{-1} (C, E = 0–1.25 V_{RHE}) and at 10 mV s^{-1} (D; 1.0–1.55 V_{RHE}) of NP deposits containing 3.4 μg Ir (0.017 mgIr cm^{-2}) and 1 wt.% Nafion on GC. The size distribution (B, inset) was determined by measuring ~100 particles.

A series of $IrNi_yO_x$ NPs were prepared using the same procedure with added $NiCl_2$. Fig. 2A plots the mass normalized (relative to Ir) activities of the GC/Ir, GC/$IrNi_{0.06}$, GC/$IrNi_{0.125}$, GC/$IrNi_{0.25}$, GC/$IrNi_{0.5}$, and GC/$IrNi_1$ oxide deposits in 0.1 M H_2SO_4. The presence of Ni increased the activity up to the atomic ratio of 8/1 Ir/Ni (GC/$IrNi_{0.125}O_x$), beyond which the activity decreased. The mass activities of GC/$IrNi_{0.5}O_x$ and GC/$IrNi_1O_x$ were ~76 and 61 A g^{-1} Ir at 1.48 V_{RHE}, respectively, significantly lower than that of GC/IrO_x (93 A g^{-1} Ir). All of these electrochemical experiments were performed at least three times to ensure reproducibility. The electrochemically active surface areas (EASAs) of the GC/IrO_x and

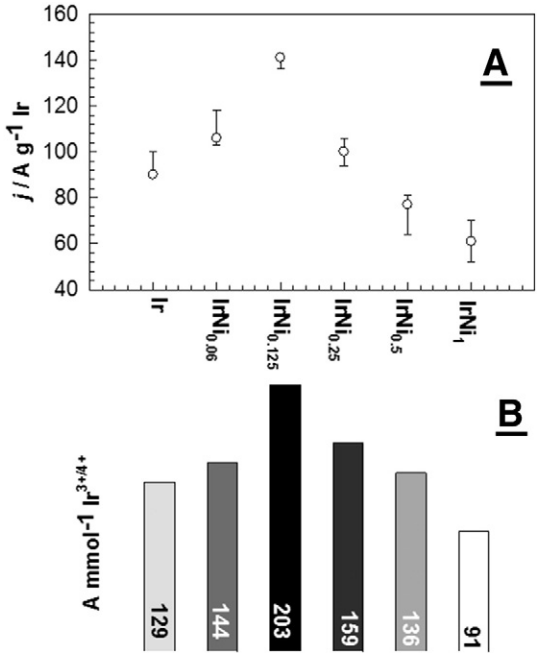

Fig. 2. A: Mass normalized activities (A g^{-1}Ir) of the IrO_x and $IrNi_yO_x$ NPs (0.017 mgIr cm^{-2}) at 1.48 V_{RHE} in 0.1 M H_2SO_4 at 10 mV s^{-1}. B: Specific activities (A $mmol^{-1}{}_{Ir}$) obtained by number of moles of Ir from the Ir electrochemistry in 0.1 M H_2SO_4.

$GC/IrNi_yO_x$ electrodes were estimated by integrating voltammetric currents over the range 0.8–1.2 V_{RHE} (corrected for the capacitive charge of the GC in 0.1 M H_2SO_4 at 10 mV s^{-1}), and assuming one electron transfer for the Ir^{3+}/Ir^{4+} redox couple [10]. Fig. 2B shows the specific activities (A $mmol^{-1}Ir^{3+/4+}$), showing nearly the same trend as the mass activity, with the $GC/IrNi_{0.125}O_x$ deposit being the most active.

Fig. 3A shows the extended anodic range voltammograms (main panel) in 0.1 M H_2SO_4 for the GC/IrO_x, $GC/IrNi_{0.125}O_x$, and GC (blank) electrodes to better illustrate the differences in WOR activity. The $GC/IrNi_{0.125}O_x$ electrode is substantially superior to the GC/IrO_x electrode over the range, whereas the onset potentials appear similar. Galvanostatic WOR at 1 mA $cm^{-2}_{geometric}$ was conducted to indicate the relative stability of these catalysts [10,11]. The GC/IrO_x and $GC/IrNi_{0.125}O_x$ electrodes produced similar durability patterns and showed no significant (over)potential increase over the measurement timescale. The potential of the $GC/IrNi_{0.125}O_x$ catalyst was offset at ~1.51 V_{RHE}, about 50 mV smaller than that of the GC/IrO_x catalyst. TEM of the $IrNi_{0.125}O_x$ in Fig. 3B shows similar particles sizes and shapes to the IrO_x (Fig. 1B). Consistently, the EASA of the GC/IrO_x and $GC/IrNi_{0.125}O_x$ electrodes are 0.578 and 0.570 cm^2 (0.396 mC cm^{-2} conversion coefficient [32]), respectively.

4. Discussion

We have shown that the as-prepared IrO_x NP can be used directly to prepare inks for WOR catalysts on GC. The WOR activity in acid of the deposited IrO_x colloid was 90 A g^{-1} Ir at 1.48 V_{RHE}, and it was considerably increased by adding Ni. The atomic ratio of Ir to Ni in the most active catalyst was 8/1 ($GC/IrNi_{0.125}O_x$), giving 140 A g^{-1} Ir at 1.48 V_{RHE}. The highest activity for an Ir/Ni catalyst reported in the literature is ~40 A g^{-1} Ir at 1.48 V_{RHE} (0.25 V overpotential). We found that catalysts with higher relative loadings of Ni were less active, and those with Ir/Ni less than 16/1 had activities similar to IrO_x. The low amount of Ni in the optimum catalyst (Ir:Ni = 8:1) suggests that Ni is not acting in a third-body effect [33]. The moderate-term stability of IrO_x and $IrNi_{0.125}O_x$ toward the galvanostatic WOR at 1 mA cm^{-2} were similar, with the $IrNi_{0.125}O_x$ operating at ~50 mV lower than that of IrO_x, and ~100 mV lower than those of the most active IrNi systems in the literature [10].

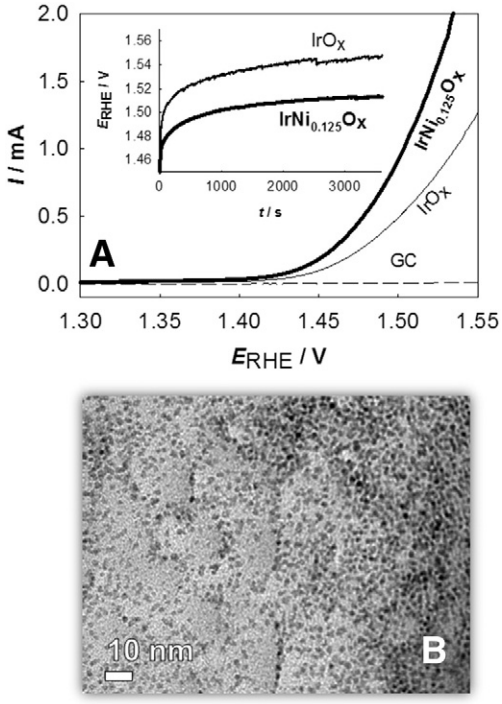

Fig. 3. A: Voltammograms (10 mV s^{-1}) for the GC, GC/IrO_x, and $GC/IrNi_{0.125}O_x$ electrodes (0.017 mgIr cm^{-2}) in 0.1 M H_2SO_4. Inset: WOR (0.087 mgIr cm^{-2}) at 1 mA $cm^{-2}_{geometric}$. B: TEM for $IrNi_{0.125}O_x$.

5. Conclusion

To our knowledge, the $IrNi_yO_x$ NPs synthesized under basic conditions in air are the most active WOR catalysts in acid reported to date [11,12], with onset potentials ~1.42 V_{RHE}, and with an optimized mass activity at 1.48 V_{RHE} ~140 A g^{-1} Ir, obtained with $IrNi_{0.125}O_x$. EASA measurements showed that the improvement in activity upon addition of Ni was not a surface area effect. Also, we suggest, based upon the low amount of Ni in the optimum catalyst (Ir:Ni = 8:1), that Ni is not acting in a third-body effect, either. Studies on the mechanism of the rate enhancement, detailed characterizations of the catalysts, and longevity studies in prototype electrolyzers are underway in our laboratories.

Acknowledgement

Authors thank Natural Sciences and Engineering Research Council of Canada (NSERC) and the University of Alberta for supporting this work. We extend gratitude to Dr. Louise Weaver in University of New Brunswick for TEM analysis.

References

[1] L.M. Peter, Electrochemical routes to earth-abundant photovoltaics: a minireview, Electrochem. Commun. 50 (2015) 88–92.
[2] E.J. Luber, J.M. Buriak, Reporting Performance in Organic Photovoltaic Devices, ACS Nano 7 (2013) 4708–4714.
[3] J.M. Buriak, Hot topics in materials chemistry and the immediacy index long-term versus short-term impact, Chem. Mater. 27 (2015) 1147–1148.
[4] S. Bensaid, G. Centi, E. Garrone, S. Perathoner, G. Saracco, Towards artificial leaves for solar hydrogen and fuels from carbon dioxide, ChemSusChem 5 (2012) 500–521.
[5] M.G. Walter, E.L. Warren, J.R. McKone, S.W. Boettcher, Q. Mi, E.A. Santori, N.S. Lewis, Solar water splitting cells, Chem. Rev. 110 (2010) 6446–6473.
[6] J. Brillet, J.-H. Yum, M. Cornuz, T. Hisatomi, R. Solarska, J. Augustynski, M. Graetzel, K. Sivula, Highly efficient water splitting by a dual-absorber tandem cell, Nat. Photonics 6 (2012) 824–828.
[7] A.J. Martín, A. Hornés, A. Martínez-Arias, L. Daza, Chapter 15—Recent advances in fuel cells for transport and stationary applications, in: L.M.G.A.M. Diéguez (Ed.), Renewable Hydrogen Technologies, Elsevier, Amsterdam 2013, pp. 361–380.
[8] J.R. Anstrom, Hydrogen as a fuel in transportation, in: A. Basile, A. Iulianelli (Eds.), Advances in Hydrogen Production, Storage and Distribution 2014, pp. 499–524.
[9] R.K. Pachauri, Y.K. Chauhan, A study, analysis and power management schemes for fuel cells, Renew. Sustain. Energy Rev. 43 (2015) 1301–1319.
[10] H.N. Nong, L. Gan, E. Willinger, D. Teschner, P. Strasser, IrOx core-shell nanocatalysts for cost- and energy-efficient electrochemical water splitting, Chem. Sci. 5 (2014) 2955–2963.
[11] H.N. Nong, H.S. Oh, T. Reier, E. Willinger, M.G. Willinger, V. Petkov, D. Teschner, P. Strasser, Oxide-supported IrNiOx core-shell particles as efficient, cost-effective, and stable catalysts for electrochemical water splitting, Angew. Chem. Int. Ed. 54 (2015) 2975–2979.
[12] H.S. Oh, H.N. Nong, T. Reier, M. Gliech, P. Strasser, Oxide-supported Ir nanodendrites with high activity and durability for the oxygen evolution reaction in acid PEM water electrolyzers, Chem. Sci. 6 (2015) 3321–3328.
[13] T. Reier, D. Teschner, T. Lunkenbein, A. Bergmann, S. Selve, R. Kraehnert, R. Schlogl, P. Strasser, Electrocatalytic oxygen evolution on iridium oxide: uncovering catalyst-substrate interactions and active iridium oxide species, J. Electrochem. Soc. 161 (2014) F876–F882.
[14] M. Carmo, D.L. Fritz, J. Mergel, D. Stolten, A comprehensive review on PEM water electrolysis, Int. J. Hydrog. Energy 38 (2013) 4901–4934.
[15] M.E.G. Lyons, R.L. Doyle, D. Fernandez, I.J. Godwin, M.P. Browne, A. Rovetta, The mechanism and kinetics of electrochemical water oxidation at oxidized metal and metal oxide electrodes. Part 1. General considerations: a mini review, Electrochem. Commun. 45 (2014) 60–62.
[16] M.E.G. Lyons, R.L. Doyle, D. Fernandez, I.J. Godwin, M.P. Browne, A. Rovetta, The mechanism and kinetics of electrochemical water oxidation at oxidized metal and metal oxide electrodes. Part 2. The surfaquo group mechanism: a mini review, Electrochem. Commun. 45 (2014) 56–59.
[17] F. Berkermann, Preparation and Application of Aqueous Iridium Oxide Colloidshttp://hdl.handle.net/11858/00-001 M-0000-000 F-8D0B-8 Ruhr-Universität Bochum, Bochum, 2010.
[18] S.W. Sheehan, J.M. Thomsen, U. Hintermair, R.H. Crabtree, G.W. Brudvig, C.A. Schmuttenmaer, A molecular catalyst for water oxidation that binds to metal oxide surfaces, Nat. Commun. 6 (2015).

[19] R. Kötz, S. Stucki, Stabilization of RuO2 by IrO2 for anodic oxygen evolution in acid media, Electrochim. Acta 31 (1986) 1311–1316.
[20] L.D. Burke, T.O. O'Meara, Oxygen electrode reaction. Part 2.-Behaviour at ruthenium black electrodes, J. Chem. Soc., Faraday Trans. 1 68 (1972) 839–848.
[21] C.C.L. McCrory, S. Jung, J.C. Peters, T.F. Jaramillo, Benchmarking heterogeneous electrocatalysts for the oxygen evolution reaction, J. Am. Chem. Soc. 135 (2013) 16977–16987.
[22] R.D.L. Smith, B. Sporinova, R.D. Fagan, S. Trudel, C.P. Berlinguette, Facile photochemical preparation of amorphous iridium oxide films for water oxidation catalysis, Chem. Mater. 26 (2014) 1654–1659.
[23] J.D. Blakemore, N.D. Schley, G.W. Olack, C.D. Incarvito, G.W. Brudvig, R.H. Crabtree, Anodic deposition of a robust iridium-based water-oxidation catalyst from organometallic precursors, Chem. Sci. 2 (2011) 94–98.
[24] J.D. Blakemore, M.W. Mara, M.N. Kushner-Lenhoff, N.D. Schley, S.J. Konezny, I. Rivalta, C.F.A. Negre, R.C. Snoeberger, O. Kokhan, J. Huang, A. Stickrath, L.A. Tran, M.L. Parr, L.X. Chen, D.M. Tiede, V.S. Batista, R.H. Crabtree, G.W. Brudvig, Characterization of an amorphous iridium water-oxidation catalyst electrodeposited from organometallic precursors, Inorg. Chem. 52 (2013) 1860–1871.
[25] C.C.L. McCrory, S. Jung, I.M. Ferrer, S.M. Chatman, J.C. Peters, T.F. Jaramillo, Benchmarking hydrogen evolving reaction and oxygen evolving reaction electrocatalysts for solar water splitting devices, J. Am. Chem. Soc. 137 (2015) 4347–4357.
[26] T. Cosgrove, Colloid Science Principles, Blackwell Publishing, Bristol, Methods and Applications, 2005.
[27] M.T. Reetz, M. Lopez, W. Grunert, W. Vogel, F. Mahlendorf, Preparation of colloidal nanoparticles of mixed metal oxides containing platinum, ruthenium, osmium, and iridium and their use as electrocatalysts, J. Phys. Chem. B 107 (2003) 7414–7419.
[28] J. Shen, H. Ziaei-Azad, N. Semagina, Is it always necessary to remove a metal nanoparticle stabilizer before catalysis? J. Mol. Catal. A Chem. 391 (2014) 36–40.
[29] Y.X. Zhao, E.A. Hernandez-Pagan, N.M. Vargas-Barbosa, J.L. Dysart, T.E. Mallouk, A high yield synthesis of ligand-free iridium oxide nanoparticles with high electrocatalytic activity, J. Phys. Chem. Lett. 2 (2011) 402–406.
[30] B.D. Sherman, S. Pillai, G. Kodis, J. Bergkamp, T.E. Mallouk, D. Gust, T.A. Moore, A.L. Moore, A porphyrin-stabilized iridium oxide water oxidation catalyst, Can. J. Chem. 89 (2011) 152–157.
[31] C. Bock, V.I. Birss, Anion and water involvement in hydrous Ir oxide redox reactions in acidic solutions, J. Electroanal. Chem. 475 (1999) 20–27.
[32] T. Pauporté, F. Andolfatto, R. Durand, Some electrocatalytic properties of anodic iridium oxide nanoparticles in acidic solution, Electrochim. Acta 45 (1999) 431–439.
[33] E. Leiva, T. Iwasita, E. Herrero, J.M. Feliu, Effect of adatoms in the electrocatalysis of HCOOH oxidation. a theoretical model, Langmuir 13 (1997) 6287–6293.